nanomaterials

MDPI

Article

Nanoimprinted and Anodized Templates for Large-Scale and Low-Cost Nanopatterning

David Navas *, David G. Trabada and Manuel Vázquez *

Instituto de Ciencia de Materiales de Madrid, ICMM-CSIC, 28049 Madrid, Spain; davidgonztra@gmail.com
* Correspondence: david.navas@csic.es (D.N.); mvazquez@icmm.csic.es (M.V.)

Abstract: Nanopatterning to fabricate advanced nanostructured materials is a widely employed technology in a broad spectrum of applications going from spintronics and nanoelectronics to nanophotonics. This work reports on an easy route for nanopatterning making use of ordered porous templates with geometries ranging from straight lines to square, triangular or rhombohedral lattices, to be employed for the designed growth of sputtered materials with engineered properties. The procedure is based on large-scale nanoimprinting using patterned low-cost commercial disks, as 1-D grating stamps, followed by a single electrochemical process that allows one to obtain 1-D ordered porous anodic templates. Multiple imprinting steps at different angles enable more complex 2-D patterned templates. Subsequently, sputtering facilitates the growth of ferromagnetic antidot thin films (e.g., from 20 to 100 nm Co thick layers) with designed symmetries. This technique constitutes a non-expensive method for massive mold production and pattern generation avoiding standard lithographical techniques. In addition, it overcomes current challenges of the two-stage electrochemical porous anodic alumina templates: (i) allowing the patterning of large areas with high ordering and/or complex antidot geometries, and (ii) being less-time consuming.

Keywords: large-scale nanopatterning; combined imprint-electrochemical processes; porous anodic alumina membranes; square and triangular 2D templates; ferromagnetic antidots

Citation: Navas, D.; Trabada, D.G.; Vázquez, M. Nanoimprinted and Anodized Templates for Large-Scale and Low-Cost Nanopatterning. *Nanomaterials* **2021**, *11*, 3430. https://doi.org/10.3390/nano11123430

Academic Editors: Chih-hung (Alex) Chang and Chang-Ho Choi

Received: 25 November 2021
Accepted: 15 December 2021
Published: 17 December 2021

1. On the State-of-the-Art of Non-Lithographic Nanopatterning

During the last decades, the use of templates has been widely exploited for the fabrication of micro- and nanostructured materials. The development of lithographic techniques has nicely allowed the achievement of nanostructures with different shapes and sizes as small as a few tens of nm [1,2]. However, they require the use of sophisticated and expensive equipment, which makes it difficult to be incorporated into the high-throughput and mass production industry. Thus, the development of more simple and less expensive fabrication methodologies for industrial procedures is a current challenge.

Templates prepared by self-assembling have been proposed as a potential alternative to overcome these limitations [3]. Among the various self-assembling methodologies, anodization is an electrochemical process that has been widely used for the fabrication of oxidized nanostructured surfaces of different materials, such as Al_2O_3 [4–6], TiO_2 [7,8], iron oxide [9,10] or SiO_2 [11,12]. In particular, porous anodic alumina (PAA) membranes were shown to be suitable for large-scale and inexpensive production of 1-, 2- and even 3-dimensional well-controlled nanotemplates [4–6,13] and with technological applicability in a broad spectrum of research and industrial fields, such as in high-density magnetic storage, solar cells, gas sensors or drug delivery [14].

Since the mid-1990s [4], PAA have been fabricated using a well-established two-step anodization process [15–19]. While the first anodization step introduces the ordering degree by performing a pre-patterning of the aluminum (Al) substrate, the second is the one in which the template thickness can be controlled. On the other hand, the anodization parameters (applied voltage, temperature and the anodic solution) are engineered to

determine the interpore distance as well as the pore diameter [16–19]. However, this self-assembled approach presents some disadvantages, such as the inability to obtain templates with neither a perfect degree of ordering at large scale nor complex geometries, and it is also a time-consuming process (up to several days).

Therefore, new and more efficient methodologies are demanded, such as hybrid nanofabrication techniques where lithographic and self-assembling methods are combined [20,21]. Among several approaches, an alternative to reach well-controlled templates consists of the mechanical nanoimprinting by which the pattern of a hard stamp (mold) is transferred onto a substrate by mechanical pressure. Nanoimprint lithography was first introduced in 1996 by Chou et al. [22], who created resist-based nanostructured templates by compressing a mold with a thin resist film, followed by an anisotropic etching to transfer the pattern through the entire template thickness.

Regarding the fabrication of PAA, this concept was successfully applied for the preparation of ordered nanoporous alumina templates after an anodization process of pre-patterned aluminum substrates that were previously imprinted by a SiC master mold prepared by electron beam lithography [23], or alternatively by Si_3N_4 [24,25] or nickel [26] master molds prepared by interference lithography. This methodology has been shown to be very effective for the preparation of defect-free alumina templates with different pore array ordering, from the standard hexagonal-array [23] to square- and triangle-array geometries [27,28]. Alternative techniques used for the pre-treatment of the Al substrate include ion-beam lithography [29], scanning probe microscopy [30], atomic force microscopy [31] and self-organized periodic array of polystyrene particles [32].

In addition, complex 2-D geometries, such as square, rectangular, rhombohedral or triangular patterns, have been successfully transferred onto different types of polymeric films using a simple 1-D grating stamp and subsequent multiple imprints [33]. There are few reports in the literature that have confirmed the possibility of applying this last approach for the fabrication of nanoporous alumina templates with different patterns employing a single lineal master mold, such as those based on a commercial optical grating [34] or a Ni line stamp [35], followed by several imprinting processes [34–36].

In this work, we introduce a non-lithographic, low-cost methodology to fabricate PAA-based large-scale templates using large nanoimprint molds followed by a single anodization process [37]. A novel aspect of this approach consists of using commercial compact discs as the imprint stamps to replicate their ordering onto the Al substrate instead of more conventional lithographic methods. Compact discs have been successfully used for different types of patterning and lithographic techniques. For example, CDs were used as imprint molds for the generation of nanostructured PMMA polymeric films [38,39] or grating-patterned TiO_2 antireflection layers for perovskite solar cells [40]. The use of CDs has even supported the generation of color patterns on various surfaces [41] or the patterning of microstructures and nanostructures of soluble materials (known as lithographically controlled wetting) [42]. Here, we have demonstrated that the patterns of these molds can be successfully transferred onto an Al substrate by single or multiple imprint processes and can achieve complex 1- or 2-dimensional well-controlled alumina templates.

These templates can be suitably employed as precursors of long-range nanopatterned structures for applications in nano-electronics, spintronics or nano-photonic devices. Here, we have prepared and studied ferromagnetic antidot thin films, grown by sputtering on these PAA templates, and with technological applicability as magnonic crystals [43,44] and magneto-plasmonic devices [45,46]. Ferromagnetic antidot arrays are nanostructures with well-defined magnetization pinning centers that affect the magnetization reversal process by controlling the nucleation and propagation of domain walls [47,48]. Additionally, a rich variety of magnetization configurations in antidot arrays have been observed whose related magnetic properties can be easily tuned by tailoring the antidot lattice symmetry [49,50], hole diameter [51] and shape [52,53], inter-hole distance [54,55], film thickness [56] and lattice defects [57]. Although most of these works were carried out by using lithographic techniques, antidot thin films with both either in-plane [58–60] or out-of-plane magnetiza-

tion easy axis [61–65] have also been reported using PAA templates. Therefore, we have grown and studied ferromagnetic antidot thin films with unconventional geometries such as linear or square structures.

In summary, we believe that our methodology, based on commercial products and conventional techniques, could be rapidly incorporated into the mass production industry with low cost and reduced time-consuming production.

2. Fabrication of Ordered Large Nanostructures by Combined Imprint and Anodization

Ordered nanostructures at large scale (up to a few cm^2) have been fabricated by combined imprint and electrochemical anodization. Figure 1 represents a schematic view of the whole process involving the imprint with a commercial stamp on a pretreated Al substrate. Imprint can be either a single- or multi-step process if subsequent imprints are performed at different angles, producing several configurations, from linear to square, triangular or rhombohedral. Afterwards, the imprint patterned Al substrates are electrochemically anodized, giving rise to ordered porous structures. In the following, we describe in further detail the different preparation steps. At the bottom of Figure 1, the great versatility of the proposed methodology for the manufacture of nanostructured porous alumina patterns is shown, summarizing the different parameters that can be used, as well as examples showing linear, square, rhombohedral and triangular configurations.

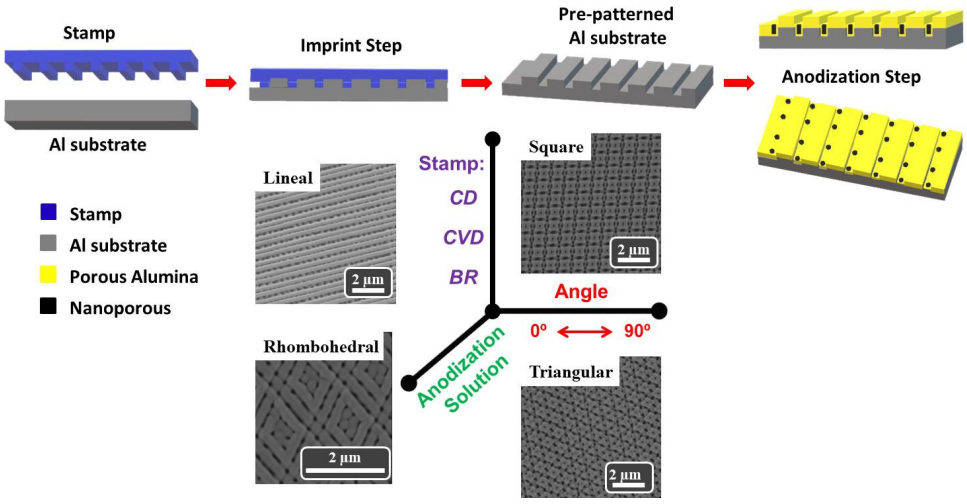

Figure 1. Schematic view summarizing the imprint and anodization processes to obtain the ordered porous nanostructured template. A general summary of the different parameters that can be used in the proposed fabrication process is shown at the bottom of the figure.

2.1. Commercial Compact Discs as Nanoimprint Molds

Commercial compact discs have been used as imprint stamps to replicate their ordering onto the Al substrate as an alternative to more conventional lithographic methods. In 1980, companies such as Philips and Sony introduced the compact disc (CD) for storing digital data. Although it is a very useful medium for recording data, demand for new media with higher storage capacity led to the development of the digital versatile disc (DVD) during the 1990s, and later to the Blu-ray (BR) disks. All these media typically consist of a 120 mm diameter polycarbonate disk with a thickness of 1.2 mm. From a general point of view, they are made up of two main patterned sections of polycarbonate. For both DVD and CD media, one of the patterned polycarbonate sections is coated with a thin reflective metallic (Al) layer. Although the reflective coating is different for BR media, its physical structure is similar to both DVD and CD. In order to obtain our patterning stamps, and according to the protocol described in References [39,66], the disks were first cut into pieces of about (3×3) cm^2. Later, commercial tape was glued to these pieces, and

the polycarbonate sections were slowly peeled off and properly cleaned using methanol (see Figure 2).

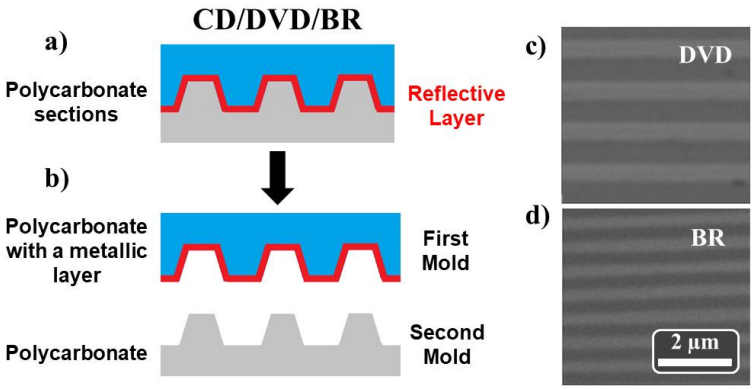

Figure 2. Schematic diagrams of the CD, DVD or BR disk media before (**a**) and after (**b**) the separation of the polycarbonate sections. SEM images of the polycarbonate stamp with a metallic layer obtained from (**c**) DVD and (**d**) BR disks.

There are several mass-produced brands offered in the market. Although available erasable/re-writable optical disks are not completely identical to each other, the clean stamps have similar linear gratings. In this work, we have used Verbatim CD and DVD [67], as well as Intenso BR [68]. Table S1, in the Supplementary Information, collects the geometrical parameters, such as the linewidth, periodicity and height, of the used optical disks. To determine the morphological properties of the nanostructures, scanning electron microscopy (SEM) analysis has been performed using a Philips XL30-FEG-SEM microscope (FEI Company, Eindhoven, Netherlands). SEM images of the polycarbonate stamps with the metallic layer, obtained from DVD and BR-disks, are shown in Figure 2c,d, respectively.

2.2. Large-Scale Imprint-Patterned Al Foils

As starting material for single and multiple imprinting steps, we considered high-purity (99.999%) Al foils (diameter and thickness of 20 mm and 0.5 mm, respectively) degreased and electrochemically polished in a mixture of perchloric acid ($HClO_4$) and ethanol (C_2H_5OH) to clean and reduce the surface roughness [17]. Afterwards, the features of the master mold were transferred to the Al substrate by an imprint process using a commercial hydraulic press and applying a pressure of 250 kg/cm^2. Multiple imprinting steps at different angles enable the transfer of more complex 2-D patterned templates, such as square or rhombohedral patterns, when a second imprint step is performed with the mold rotated by an angle of 90° or 60°, respectively.

Figure 3 shows SEM images of the line arrays generated on the Al substrate after an imprint process using molds based on CD, DVD or BR disks, respectively. In agreement with the optical disks' geometrical properties (described in Table S1 in the Supplementary Information), the patterned Al substrates present periodicities of around 1600, 740 or 320 nm (see Figure 3a–c, respectively).

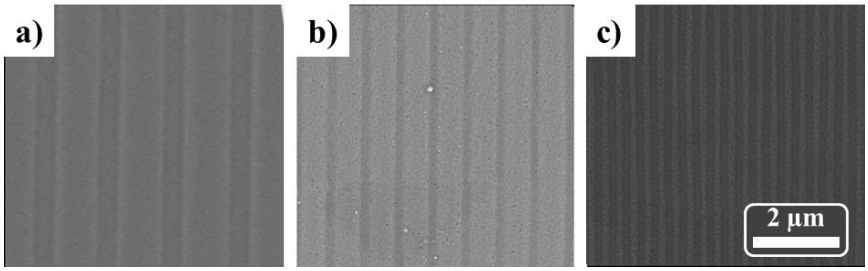

Figure 3. SEM images of stripe patterns on the Al substrate after one imprint step using CD-PS/ML (**a**), DVD-PS/ML (**b**) and BR-PS/ML (**c**) molds.

Square-based patterns can also be achieved when a second imprint step is performed with the mold rotated by an angle of 90° (examples are shown in Figure 4a–c). More complex patterns, such as rectangular (Figure 4d) or rhombohedral geometries (Figure 4e), can be produced by using different molds for each imprint step and when the mold is rotated for the second imprint process by 90° or 60°, respectively. Although we are using polymeric molds, we have made several imprints without the mold being degraded and/or destroyed by the applied pressure.

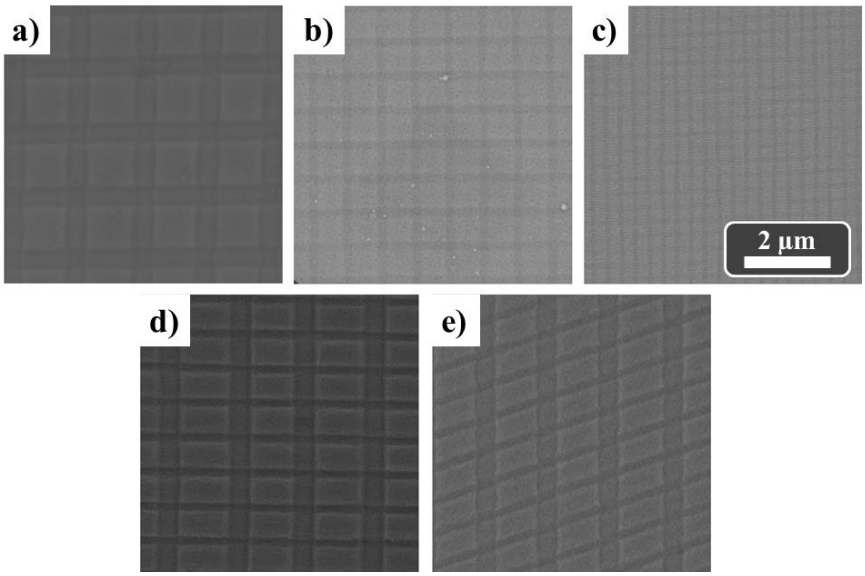

Figure 4. SEM images of square patterns on the Al substrate after two imprint steps using CD-PS/ML (**a**), DVD-PS/ML (**b**) and BR-PS/ML (**c**) molds. SEM images of rectangular and rhombohedral patterns on Al substrate after two imprint steps combining CD- PS/ML and DVD- PS/ML molds and when the mold was rotated for the second imprint process by 90° (**d**) and 60° (**e**).

2.3. PAA Nanostructures Grown by Anodization of Imprint-Patterned Al Foils

After the single- or multi-imprint process, a single anodization step was conducted under a constant voltage of 195 V in 0.03 M phosphoric acid (H_3PO_4) solution at a temperature of 5° C for 2 h. We observed that the anodization process in such a diluted phosphoric acid-based solution, and for time $\leq$2 h, did not significantly alter the configuration of the pre-patterned aluminum foil.

As indicated above, three stamps, namely CD-PS/ML, DVD-PS/ML and BR-PS/ML molds, were employed. As an example, we focus on the results obtained using DVD-PS/ML mold while similar data were observed when CD-PS/ML or BR-PS/ML molds were used (see for example Figure S1 in the Supplementary Information). Figure 5 shows SEM images of the PAA nanostructured templates after a single anodization step of Al substrates pre-patterned using a DVD-PS/ML mold, with stripe, square and triangular geometries.

PAAs with a single-imprint process exhibit two main regions (Figure 5a–c): the alumina grown in the highest sections of the pre-patterned Al substrate show the formation of a continuous line due to the collapse of the pores (or frustrated pores), while the second region shows a well-aligned line of pores with an average pore diameter of ≈200 nm. A closer inspection at the cross-section SEM image (Figure 5c) shows that these well-aligned pores transform into two pores along alumina template thickness.

On the other hand, multi-imprint steps allow the achievement of more complex geometries. Two-imprint steps generate a well-ordered pore array with square configuration when the mold was rotated by an angle of 90° between imprints (Figure 5d–f). It was observed that PAA nanostructured templates with a single pore, with an average diameter of ≈70 nm, grew within each square of ≈500 nm lateral sizes. Finally, three-imprint steps,

where the mold was rotated by an angle of 60° between imprints, were able to generate a triangular configuration with a more complex pore distribution (see Figure 5g–i).

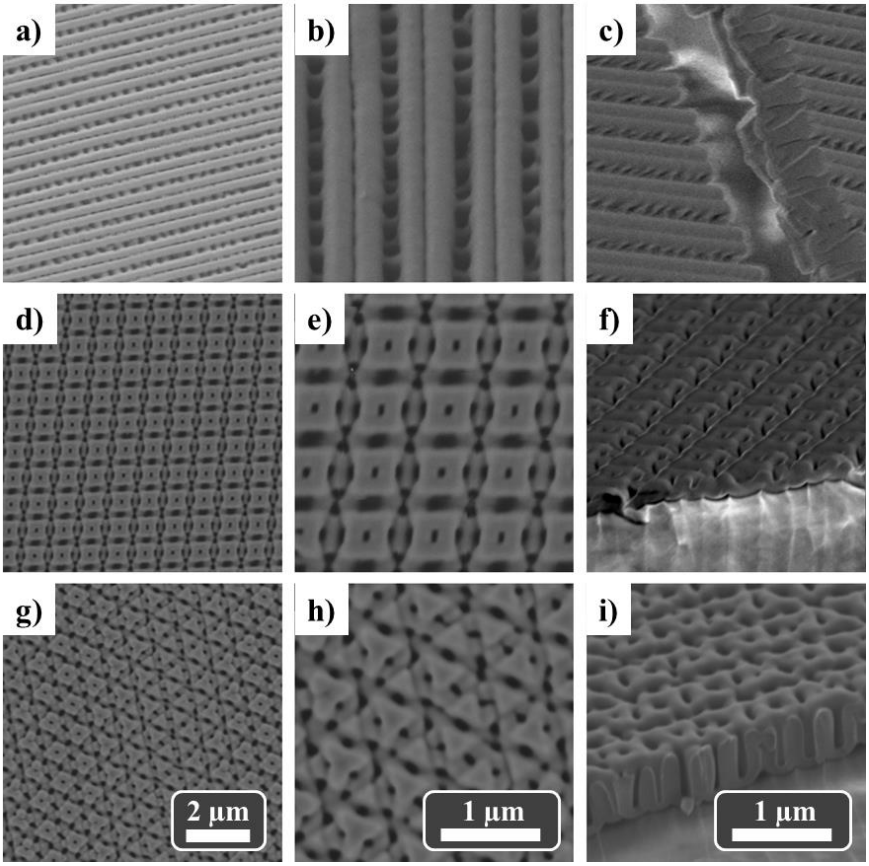

Figure 5. Top-view (**a**,**b**,**d**,**e**,**g**,**h**) and cross-section (**c**,**f**,**i**) SEM images of PAA templates with line (**a**–**c**), square (**d**–**f**) and triangular configurations (**g**–**i**) imprinted using DVD-PS/ML molds and a single anodization step under constant voltage of 195 V in 0.03M H_3PO_4 solution at 5 °C and for 2 h.

In order to check the influence of the experimental conditions, the same pre-patterned Al substrates were also anodized under a lower constant voltage (165 V) in 0.03M H_3PO_4 solution at 5 °C and for 2 h. PAA templates with very similar morphologies were obtained (see Figure S2 in the Supplementary Information), confirming that the final configuration of the PAA templates is mainly controlled by the geometry of the pre-patterned Al substrates.

3. Sputtering Ordered Co Nanostructures on Imprint-Anodic PAA Templates

The described imprint-anodic samples can be used as templates for the generation of various nanostructures with encoded ordering for a wide spectrum of applications. As a particular example, we address the case of several Co antidot thin films and their overall magnetic characterization of interest for applications. Therefore, after the anodization process, the PAA nanostructured templates were coated with a Co layer using a home-made rf sputtering system. The Ar (99.999% pure) sputtering gas pressure was fixed to 1.2×10^{-2} mbar, the base pressure was below 2.5×10^{-4} mbar, and the power applied was 99 W for the 5 cm diameter target. Under these experimental conditions, the Co deposition rate was 3.1 nm/s. Three samples were prepared with 20, 50 and 100 nm thicknesses, respectively.

3.1. Morphology and Structural Characterization of Ordered Co Nanostripes and Square Arrays

The SEM images in Figure 6a,b correspond to the 50 nm thick sputtered Co sample. Longitudinal Co double-nanostripe structures are observed, showing a lateral periodical

modulation replicating the previously imposed ordering of the anodic PAA nanostructure (shown in Figure 5a–c). The modulation is interpreted to be a consequence of the anodization process in connection with the observed transversal understructure (see Figure 6b) that corresponds to the Co growth on the groove zones connecting the Co double-nanostripe structures.

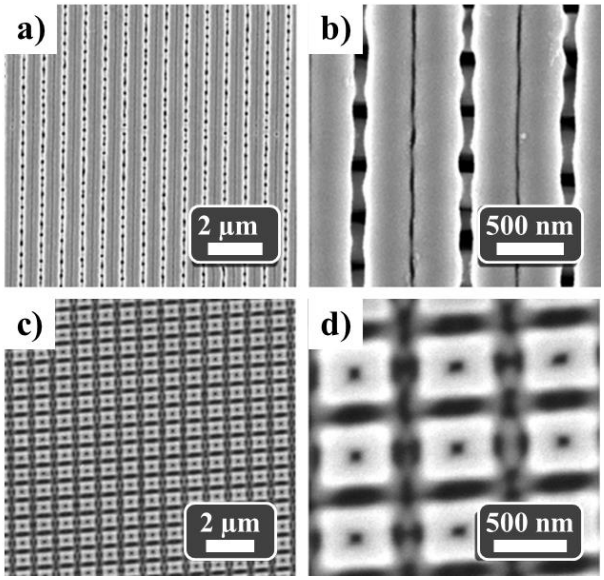

Figure 6. Top-view SEM images of (**a**,**b**) an array of Co double-nanostripes and (**c**,**d**) Co squares in a cubic arrangement (50 nm thick Co antidot films in both cases).

In order to grow ordered arrays of Co squares with cubic symmetry, we used the ordered nanostructured templates shown in Figure 5d–f. Then, the Co layer was sputtered onto them in a similar way as it was previously described. Figure 6c,d shows SEM images of the 50 nm thick Co squared dot array. Nanodots take near-squared shape (520×520 nm^2), separated by around 220 nm with a pore at the center and a macroscopic squared arrangement. As it was observed in the case of Co nanostripes, we note that neighboring Co squared nanodots are connected by a Co understructure. This is confirmed in Figure S3 (Supplementary Information) where a freestanding nanoporous Co membrane was obtained after the chemical dissolution from the PAA template.

Microstructural characterization of ordered Co nanostructures was performed by X-ray diffraction (XRD) using a Bruker D8 Advance diffractometer (Bruker, Billerica, MA, USA) with Cu Kα radiation (λ = 1.540593 Å). The diffraction pattern (see Figure S4 in the Supplementary Information for additional details) shows three well-defined peaks corresponding to Al (220) and (311), as well as to Co at $2\theta \approx 43.74^\circ$. Since the fcc Co (1 1 1) reflection ($2\theta = 44.571^\circ$) [69] is close to the hcp Co (0 0 0 2) reflection ($2\theta = 44.949^\circ$) [70], the crystallographic phase of the Co layer cannot be resolved. Then, we suggest that the Co layer is polycrystalline and crystallized in hcp phase with (0 0 0 1) texture or fcc with (1 1 1) texture.

3.2. Magnetic Characterization of Ordered Co Nanostripes and Co Square Arrays

The magnetic characterization of these Co nanostructures was carried out at room temperature using a vibrating sample magnetometer (VSM, model KLA-Tencor EV7, KLA-Tencor Corporation, Westwood, MA, USA). The VSM experimental setup allowed the rotation of the sample so that it was possible to determine the azimuthal (in-plane) angular dependence under a maximum magnetic field of $\pm$18 kOe.

As it was previously described [71], the in-plane magnetization reversal of a Co thin film mostly proceeds by the nucleation and propagation of domain walls, resulting in nearly square hysteresis loops and coercivity fields of $\approx$30 Oe. Figure 7 shows the azimuthal

angular dependence of the hysteresis loops for the Co double-nanostripes with thickness of 20 (Figure 7a–c), 50 (Figure 7d–f) and 100 nm (Figure 7g–i). In all of them, the hysteresis loops, M/Ms vs. H, also show a nearly square shape with a single giant Barkhausen jump for a configuration of the applied field parallel to the nanostripes (0°). The loops evolve progressively to S-shaped with decreasing susceptibility as the orientation of the magnetic field rotates towards the perpendicular orientation (90°). The measurements indicate that maximum coercivity, H_c, and reduced remanence, M_r/M_s, values are observed nearly along the direction parallel to the nanostripes, indicating that this corresponds to the magnetization easy axis in these three samples. The perpendicular orientation of the applied field roughly corresponds to a magnetization hard axis.

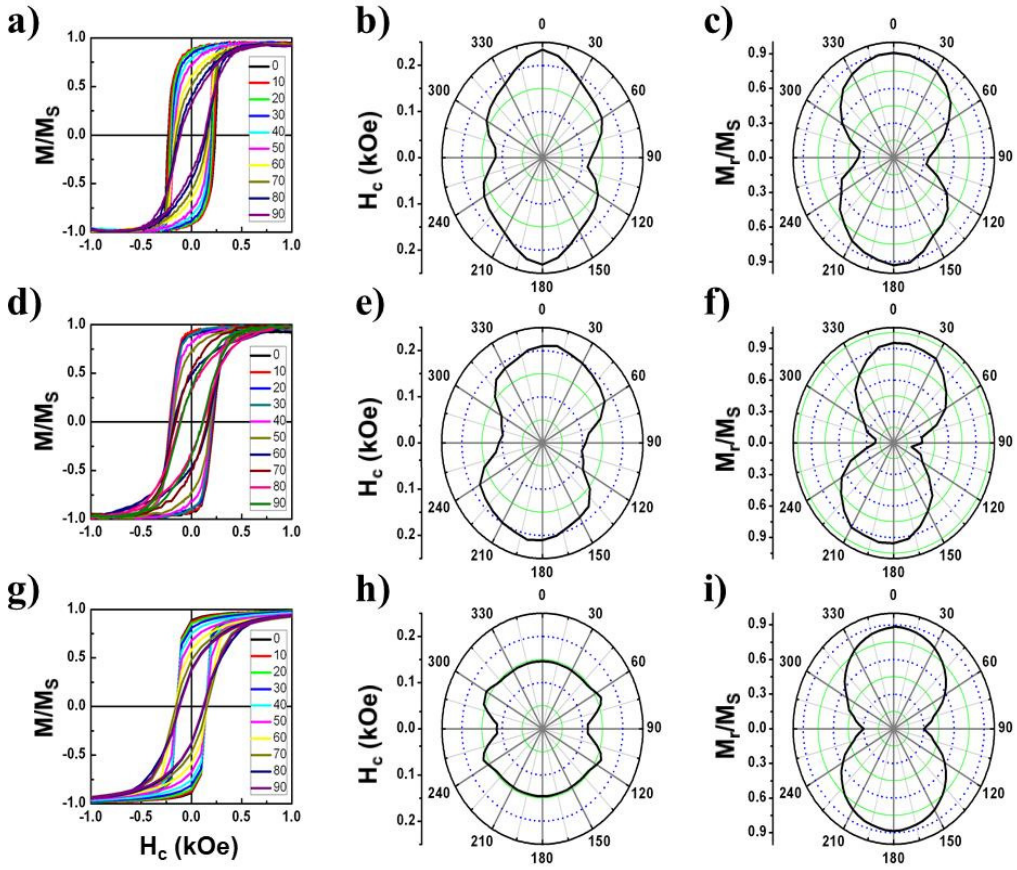

Figure 7. In-plane azimuthal VSM hysteresis loops, M/Ms, of ordered Co double-nanostripes with 20 (**a**), 50 (**d**) and 100 nm (**g**) Co thick. The corresponding angular dependence of coercivity, Hc, and reduced remanence, Mr/Ms, are given in (**b**,**e**,**h**) and (**c**,**f**,**i**), respectively. The reference 0° corresponds to parallel alignment of the applied field with the nanostripe main axis.

The angular dependence of coercivity for the 20 nm (Figure 7b) and 50 nm (Figure 7e) thick nanostripes can be interpreted assuming a strong, nearly uniaxial shape anisotropy originating in the high length-to-thickness aspect ratio of the nanostripes. However, an additional anisotropic term should be considered to understand the local angular coercivity maxima at around 60° and 120°. This effect is even more pronounced in the case of thicker nanostripes (100 nm thick) where the coercivity angular profile particularly reduces its anisotropic behavior (see Figure 7h). The occurrence of such multiple secondary maximum values for the coercivity indicates that the anisotropy is not fully uniaxial but contains a four-fold anisotropy. The origin for that four-fold symmetry seems to originate from the presence of the Co transversal understructures. Note however that for the reduced remanence angular profile (Figure 7c,f,i), such four-fold anisotropy is less apparent.

A preliminary magnetic characterization was also carried out in the Co squared nanodots arrays (see Figure S5 in the Supplementary Information). There, we observe a less remarkable angular dependence, which is related to a less defined shape anisotropy term. A deeper analysis of the angular dependence of coercivity and reduced remanence suggests the presence of a modest in-plane bi-axial magnetic anisotropy with magnetization easy axes at 90° to each other. The in-plane bi-axial magnetic anisotropy seems to be related to the cubic array of squared Co nanodots. Further analysis of complex geometrical nanostructures will be detailed in the future.

4. Conclusions

In summary, the main objective of this work has been the development of a methodology for the fabrication of large-scale and low-cost PAA nanostructured templates with well-defined order and versatile complex geometries. The procedure consists of a first step by which the ordering of commercially standard stamps such as CD, DVD and BR disks is transferred into Al foils. It is followed by an electrochemical single anodization process resulting in nanostructured porous ordered alumina templates. Moreover, it was demonstrated that complex 2-D template structures can be produced from 1-D stamps by multiple imprinting steps at different angles. This low time-consuming and inexpensive technique makes such nanostructured templates suitable for a gentle incorporation into the high-throughput and mass production industry.

These PAA nanostructures can be further used as templates to grow specific geometrical nanostructures such as arrays of nanostripes or squared/rombohedral ordered nanostructures. In particular, a specific study has been performed on ordered Co nanostripe thin films and squared dot arrays. It was confirmed that the magnetic behaviour of the sputtered antidot thin films mainly depends on the shape anisotropy contribution and can be engineered by the appropriate nanoimprint processes.

Therefore, the proposed technique constitutes a non-expensive method for massive mold production and pattern generation avoiding standard lithographical techniques [32]. A number of technologies, such as nano-photonic and nano-electronic devices, are expected to profit from this simple and cost-effective fabrication methodology.

Supplementary Materials: The following are available online at https://www.mdpi.com/article/10.3390/nano11123430/s1, Table S1: The geometrical parameters, such as periodicity, linewidth, line height, and mold thickness, of the commercial optical disks employed as molds for the imprint step, Figure S1: SEM images of the PAA nanostructured templates, after a single anodization step of Al substrates and pre-patterned using a CD-PS/ML mold, Figure S2: SEM images of PAA nanostructured templates with line (a and b), square (c,d) and triangular (e,f) geometrical configurations imprinted using DVD-PS/ML molds and a single anodization step under constant voltage of 165 V in 0.03M H_3PO_4 solution at 5 °C and for 2 h, Figure S3: SEM images of a free-standing square Co nanostructure after the chemical dissolution of the PAA template, Figure S4: XRD patterns of the Co thin films sputtered onto the PAA templates, Figure S5: The in-plane angular dependence of the VSM hysteresis loops for the Co nanodot array (a) as well as its in-plane coercivity (b) and reduced remanence (c). Reference [72] is cited in supplementary materials.

Author Contributions: Conceptualization, D.G.T. and M.V.; methodology, D.G.T. and M.V.; validation, D.N., D.G.T. and M.V.; formal analysis, D.N. and M.V.; investigation, D.G.T.; resources, D.N. and M.V.; writing—original draft preparation, D.G.T.; writing—review and editing, D.N. and M.V.; supervision, D.N. and M.V.; project administration, M.V.; funding acquisition, M.V. All authors have read and agreed to the published version of the manuscript.

Funding: This research was funded by the SPANISH MINISTRY OF ECONOMY AND COMPETITIVENESS (MINECO) under the projects MAT2013-48054-C2-1-R and PID2019-108075RB-C31, and the REGIONAL GOVERNMENT OF MADRID under Project S2018/NMT-4321 (NANOMAGCOST-CM). DN wants to acknowledge the grant RYC-2017-22820 funded by MCIN/AEI/10.13039/501100011033 and by "ESF Investing in your future".

Institutional Review Board Statement: Not applicable.

Informed Consent Statement: Not applicable.

Data Availability Statement: The data presented in this study are available on request from the corresponding author.

Conflicts of Interest: The authors declare no conflict of interest.

References

1. Pease, R.F.; Chou, S.Y. Lithography and Other Patterning Techniques for Future Electronics. *Proc. IEEE* **2008**, *96*, 248–270. [CrossRef]
2. Ito, T.; Okazaki, S. Pushing the limits of lithography. *Nature* **2000**, *406*, 1027–1031. [CrossRef] [PubMed]
3. Whitesides, G.M.; Grzybowski, B. Self-Assembly at All Scales. *Science* **2002**, *295*, 2418–2421. [CrossRef] [PubMed]
4. Masuda, H.; Fukuda, K. Ordered Metal Nanohole Arrays Made by a Two-Step Replication of Honeycomb Structures of Anodic Alumina. *Science* **1995**, *268*, 1466–1468. [CrossRef]
5. Lee, W.; Ji, R.; Gosele, U.; Nielsch, K. Fast fabrication of long-range ordered porous alumina membranes by hard anodization. *Nat. Mater.* **2006**, *5*, 741–747. [CrossRef]
6. Losic, D.; Losic, D. Preparation of Porous Anodic Alumina with Periodically Perforated Pores. *Langmuir* **2009**, *25*, 5426–5431. [CrossRef]
7. Roy, P.; Berger, S.; Schmuki, P. TiO_2 Nanotubes: Synthesis and Applications. *Angew. Chem. Int. Ed.* **2011**, *50*, 2904–2939. [CrossRef]
8. Li, Z.; Xin, Y.; Zhang, Z. Colorful titanium oxides: A new class of photonic materials. *Nanoscale* **2015**, *7*, 19894. [CrossRef]
9. Mohapatra, S.K.; John, S.E.; Banerjee, S.; Misra, M. Water Photooxidation by Smooth and Ultrathin r-Fe_2O_3 Nanotube Arrays. *Chem. Mater.* **2009**, *21*, 3048–3055. [CrossRef]
10. Kang, J.S.; Noh, Y.; Kim, J.; Choi, H.; Jeon, T.H.; Ahn, D.; Kim, J.-Y.; Yu, S.-H.; Park, H.; Yum, J.-H.; et al. Iron Oxide Photoelectrode with Multidimensional Architecture for Highly Efficient Photoelectrochemical Water Splitting. *Angew. Chem. Int. Ed.* **2017**, *56*, 6583–6588. [CrossRef]
11. Albonetti, C.; Barbalinardo, M.; Milita, S.; Cavallini, M.; Liscio, F.; Moulin, J.-F.; Biscarini, F. Selective Growth of α-Sexithiophene by Using Silicon Oxides Patterns. *Int. J. Mol. Sci.* **2011**, *12*, 5719–5735. [CrossRef] [PubMed]
12. Cavallini, M.; Hemmatian, Z.; Riminucci, A.; Prezioso, M.; Morandi, V.; Murgia, M. Regenerable Resistive Switching in Silicon Oxide Based Nanojunctions. *Adv. Mater.* **2012**, *24*, 1197–1201. [CrossRef]
13. Martín, J.; Martín-González, M.; Fernández, J.F.; Caballero-Calero, O. Ordered three-dimensional interconnected nanoarchitectures in anodic porous alumina. *Nat. Commun.* **2014**, *5*, 5130. [CrossRef]
14. Sousa, C.T.; Leitao, D.C.; Proenca, M.P.; Ventura, J.; Pereira, A.M.; Araujo, J.P. Nanoporous alumina as templates for multifunctional applications. *Appl. Phys. Rev.* **2014**, *1*, 031102. [CrossRef]
15. Nielsch, K.; Choi, J.; Schwirn, K.; Wehrspohn, R.B.; Gosele, U. Self-ordering Regimes of Porous Alumina: The 10 Porosity Rule. *Nano Lett.* **2002**, *2*, 677–680. [CrossRef]
16. Jessensky, O.; Muller, F.; Gosele, U. Self-organized formation of hexagonal pore arrays in anodic alumina. *Appl. Phys. Lett.* **1998**, *72*, 1173. [CrossRef]
17. Li, A.P.; Muller, F.; Birner, A.; Nielsch, K.; Gosele, U. Hexagonal pore arrays with a 50–420 nm interpore distance formed by self-organization in anodic alumina. *J. Appl. Phys.* **1998**, *84*, 6023–6026. [CrossRef]
18. Li, A.-P.; Müller, F.; Birner, A.; Nielsch, K.; Gösele, U. Fabrication and Microstructuring of Hexagonally Ordered Two-Dimensional Nanopore Arrays in Anodic Alumina. *Adv. Mater.* **1999**, *11*, 483–487. [CrossRef]
19. Li, F.; Zhang, L.; Metzger, R.M. On the Growth of Highly Ordered Pores in Anodized Aluminum Oxide. *Chem. Mater.* **1998**, *10*, 2470–2480. [CrossRef]
20. Biswas, A.; Bayer, I.S.; Biris, A.S.; Wang, T.; Dervishi, E.; Faupel, F. Advances in top–down and bottom–up surface nanofabrication: Techniques, applications & future prospects. *Adv. Colloid Interface Sci.* **2012**, *170*, 2–27. [CrossRef] [PubMed]
21. Cheng, J.Y.; Ross, C.A.; Smith, H.I.; Thomas, E.L. Templated Self-Assembly of Block Copolymers: Top-Down Helps Bottom-Up. *Adv. Mater.* **2006**, *18*, 2505–2521. [CrossRef]
22. Chou, S.Y.; Krauss, P.R.; Renstrom, P.J. Imprint Lithography with 25-Nanometer Resolution. *Science* **1996**, *272*, 85–87. [CrossRef]
23. Masuda, H.; Yamada, H.; Satoh, M.; Asoh, H.; Nakao, M.; Tamamura, T. Highly ordered nanochannel-array architecture in anodic alumina. *Appl. Phys. Lett.* **1997**, *71*, 2770–2772. [CrossRef]
24. Choi, J.; Schilling, J.; Nielsch, K.; Hillebrand, R.; Reiche, M.; Wehrspohn, R.B.; Gösele, U. Large-area porous alumina photonic crystals via imprint method. *MRS Online Proc. Libr.* **2002**, *722*, 52. [CrossRef]
25. Choi, J.; Nielsch, K.; Reiche, M.; Wehrspohn, R.B.; Gösele, U. Fabrication of monodomain alumina pore arrays with an interpore distance smaller than the lattice constant of the imprint stamp. *J. Vac. Sci. Technol. B* **2003**, *21*, 763–766. [CrossRef]
26. Lee, W.; Ji, R.; Ross, C.A.; Gosele, U.; Nielsch, K. Wafer-Scale Ni Imprint Stamps for Porous Alumina Membranes Based on Interference Lithography. *Small* **2006**, *2*, 978–982. [CrossRef] [PubMed]
27. Asoh, H.; Ono, S.; Hirose, T.; Nakao, M.; Masuda, H. Growth of anodic porous alumina with square cells. *Electrochim. Acta* **2003**, *48*, 3171–3174. [CrossRef]
28. Masuda, H.; Asoh, H.; Watanabe, M.; Nishio, K.; Nakao, M.; Tamamura, T. Square and Triangular Nanohole Array Architectures in Anodic Alumina. *Adv. Mater.* **2001**, *13*, 189–192. [CrossRef]

29. Liu, N.W.; Datta, A.; Liu, C.Y.; Wang, Y.L. High-speed focused-ion-beam patterning for guiding the growth of anodic alumina nanochannel arrays. *Appl. Phys. Lett.* **2003**, *82*, 1281–1283. [CrossRef]
30. Masuda, H.; Kanezawa, K.; Nishio, K. Fabrication of Ideally Ordered Nanohole Arrays in Anodic Porous Alumina Based on Nanoindentation Using Scanning Probe Microscope. *Chem. Lett.* **2002**, *31*, 1218–1219. [CrossRef]
31. Jaafar, M.; Navas, D.; Hernández-Vélez, M.; Baldonedo, J.L.; Vázquez, M.; Asenjo, A. Nanoporous alumina membrane prepared by nanoindentation and anodic oxidation. *Surf. Sci.* **2009**, *603*, 3155–3159. [CrossRef]
32. Hideki, M.; Yoshitaka, M.; Masato, Y.; Futoshi, M.; Kazuyuki, N. Fabrication of Highly Ordered Anodic Porous Alumina Using Self-organized Polystyrene Particle Array. *Chem. Lett.* **2004**, *33*, 584–585. [CrossRef]
33. Mukherjee, R.; Sharma, A.; Patil, G.; Faruqui, D.; Sarathi, P.; Pattader, G. Soft lithography meets self-organization: Some new developments in meso-patterning. *Bull. Mater. Sci.* **2008**, *31*, 249–261. [CrossRef]
34. Mikulskas, I.; Juodkazis, S.; Tomasiunas, R.; Dumas, J.G. Aluminum Oxide Photonic Crystals Grown by a New Hybrid Method. *Adv. Mater.* **2001**, *13*, 1574–1577. [CrossRef]
35. Sung, S.-Y.; Maqableh, M.M.; Huang, X.; Sai Madhukar Reddy, K.; Victora, R.H.; Stadler, B.J.H. Metallic 10 nm Diameter Magnetic Sensors and Large-Scale Ordered Arrays. *IEEE Trans. Magn.* **2014**, *50*, 3303705. [CrossRef]
36. Choi, J.; Wehrspohn, R.B.; Gösele, A. Moiré Pattern Formation on Porous Alumina Arrays Using Nanoimprint Lithography. *Adv. Mater.* **2003**, *15*, 1531–1534. [CrossRef]
37. Vazquez, M.; Trabada, D.G.; Navas, D. Method for Nanostructured Materials Fabrication Combining Soft Lithographic Imprint, Aluminum Anodization and Metal Sputtering. EU Patent PCT/EP2020/066600, 16 June 2020.
38. Baquedano, E.; Torné, L.; Caño, P.; Postigo, P.A. Increased Efficiency of Solar Cells Protected by Hydrophobic and Hydrophilic Anti-Reflecting Nanostructured Glasses. *Nanomaterials* **2017**, *7*, 437. [CrossRef]
39. Song, J.; Lu, H.; Li, S.; Tan, L.; Gruverman, A.; Ducharme, S. Fabrication of ferroelectric polymer nanostructures on flexible substrates by soft-mold reverse nanoimprint lithography. *Nanotechnology* **2016**, *27*, 015302. [CrossRef]
40. Deng, K.; Liu, Z.; Wang, M.; Li, L. Nanoimprinted Grating-Embedded Perovskite Solar Cells with Improved Light Management. *Adv. Funct. Mater.* **2019**, *29*, 1900830. [CrossRef]
41. Chowdhury, D.; Paul, A.; Chattopadhyay, A. Patterning Design in Color at the Submicron Scale. *Nano Lett.* **2001**, *1*, 409–412. [CrossRef]
42. Cavallini, M.; Gentili, D.; Greco, P.; Valle, F.; Biscarini, F. Micro- and nanopatterning by lithographically controlled wetting. *Nat. Protoc.* **2012**, *7*, 1668–1676. [CrossRef] [PubMed]
43. Krawczyk, M.; Grundler, D. Review and prospects of magnonic crystals and devices with reprogrammable band structure. *J. Phys. Condens. Matter* **2014**, *26*, 123202. [CrossRef]
44. Neusser, S.; Grundler, D. Magnonics: Spin Waves on the Nanoscale. *Adv. Mater.* **2009**, *21*, 2927–2932. [CrossRef]
45. Ctistis, G.; Papaioannou, E.; Patoka, P.; Gutek, J.; Fumagalli, P.; Giersig, M. Optical and Magnetic Properties of Hexagonal Arrays of Subwavelength Holes in Optically Thin Cobalt Films. *Nano Lett.* **2009**, *9*, 1–6. [CrossRef] [PubMed]
46. González-Díaz, J.B.; García-Martín, J.M.; García-Martín, A.; Navas, D.; Asenjo, A.; Vázquez, M.; Hernández-Vélez, M.; Armelles, G. Plasmon-enhanced magneto-optical activity in ferromagnetic membranes. *Appl. Phys. Lett.* **2009**, *94*, 263101. [CrossRef]
47. Cowburn, R.P.; Adeyeye, A.O.; Bland, J.A.C. Magnetic domain formation in lithographically defined antidot Permalloy arrays. *Appl. Phys. Lett.* **1997**, *70*, 2309–2311. [CrossRef]
48. Torres, L.; Lopez-Diaz, L.; Iñiguez, J. Micromagnetic tailoring of periodic antidot permalloy arrays for high density storage. *Appl. Phys. Lett.* **1998**, *73*, 3766–3768. [CrossRef]
49. Tacchi, S.; Madami, M.; Gubbiotti, G.; Carlotti, G.; Adeyeye, A.O.; Neusser, S.; Botters, B.; Grundler, D. Angular Dependence of Magnetic Normal Modes in NiFe Antidot Lattices with Different Lattice Symmetry. *IEEE Trans. Magn.* **2010**, *46*, 1440–1443. [CrossRef]
50. Vavassori, P.; Gubbiotti, G.; Zangari, G.; Yu, C.T.; Yin, H.; Jiang, H.; Mankey, G.J. Lattice symmetry and magnetization reversal in micron-size antidot arrays in Permalloy film. *J. Appl. Phys.* **2002**, *91*, 7992–7994. [CrossRef]
51. Ding, J.; Tripathy, D.; Adeyeye, A.O. Effect of antidot diameter on the dynamic response of nanoscale antidot arrays. *J. Appl. Phys.* **2011**, *109*, 07D304. [CrossRef]
52. Tse, D.H.Y.; Steinmuller, S.J.; Trypiniotis, T.; Anderson, D.; Jones, G.A.C.; Bland, J.A.C.; Barnes, C.H.W. Static and dynamic magnetic properties of Ni80Fe20 square antidot arrays. *Phys. Rev. B* **2009**, *79*, 054426. [CrossRef]
53. Mandal, R.; Laha, P.; Das, K.; Saha, S.; Barman, S.; Raychaudhuri, A.K.; Barman, A. Effects of antidot shape on the spin wave spectra of two-dimensional $Ni_{80}Fe_{20}$ antidot lattices. *Appl. Phys. Lett.* **2013**, *103*, 262410. [CrossRef]
54. Yu, C.; Pechan, M.J.; Mankey, G.J. Dipolar induced, spatially localized resonance in magnetic antidot array. *Appl. Phys. Lett.* **2003**, *83*, 3948–3950. [CrossRef]
55. Martyanov, O.N.; Yudanov, V.F.; Lee, R.N.; Nepijko, S.A.; Elmers, H.J.; Hertel, R.; Schneider, C.M.; Schönhense, G. Ferromagnetic resonance study of thin film antidot arrays: Experiment and micromagnetic simulations. *Phys. Rev. B* **2007**, *75*, 174429. [CrossRef]
56. Vovk, A.; Golub, V.; Salyuk, O.; Krivoruchko, V.N.; Marchenko, A.I. Evolution of the ferromagnetic resonance spectrum of a hexagonal antidot lattice with film thickness: Experiment and numerical simulations. *J. Appl. Phys.* **2015**, *117*, 073903. [CrossRef]
57. Manzin, A.; Barrera, G.; Celegato, F.; Coïsson, M.; Tiberto, P. Influence of lattice defects on the ferromagnetic resonance behaviour of 2D magnonic crystals. *Sci. Rep.* **2016**, *6*, 22004. [CrossRef] [PubMed]

58. Yanagishita, T.; Nishio, K.; Masuda, H. Fabrication of Metal Nanohole Arrays with High Aspect Ratios Using Two-Step Replication of Anodic Porous Alumina. *Adv. Mater.* **2005**, *17*, 2241–2243. [CrossRef]
59. Lei, Y.; Chim, W.-K.; Zhang, Z.; Zhou, T.; Zhang, L.; Meng, G.; Phillipp, F. Ordered nanoporous nickel films and their magnetic properties. *Chem. Phys. Lett.* **2003**, *380*, 313–318. [CrossRef]
60. Navas, D.; Hernández-Vélez, M.; Vázquez, M.; Lee, W.; Nielsch, K. Ordered Ni nanohole arrays with engineered geometrical aspects and magnetic anisotropy. *Appl. Phys. Lett.* **2007**, *90*, 192501. [CrossRef]
61. Rahman, M.T.; Shams, N.N.; Wu, Y.-C.; Lai, C.-H.; Suess, D. Magnetic multilayers on porous anodized alumina for percolated perpendicular media. *Appl. Phys. Lett.* **2007**, *91*, 132505. [CrossRef]
62. Navas, D.; Ilievski, F.; Ross, C.A. CoCrPt antidot arrays with perpendicular magnetic anisotropy made on anodic alumina templates. *J. Appl. Phys.* **2009**, *105*, 113921. [CrossRef]
63. Tofizur Rahman, M.; Dumas, R.K.; Eibagi, N.; Shams, N.N.; Wu, Y.-C.; Liu, K.; Lai, C.-H. Controlling magnetization reversal in Co/Pt nanostructures with perpendicular anisotropy. *Appl. Phys. Lett.* **2009**, *94*, 042507. [CrossRef]
64. Salaheldeen, M.; Méndez, M.; Vega, V.; Fernández, A.; Prida, V.M. Tuning Nanohole Sizes in Ni Hexagonal Antidot Arrays: Large Perpendicular Magnetic Anisotropy for Spintronic Applications. *ACS Appl. Nano Mater.* **2019**, *2*, 1866–1875. [CrossRef]
65. Salaheldeen, M.; Vega, V.; Caballero-Flores, R.; Prida, V.M.; Fernández, A. Influence of nanoholes array geometrical parameters on magnetic properties of Dy–Fe antidot thin films. *Nanotechnology* **2019**, *30*, 455703. [CrossRef]
66. Prakash, T. Submicron Size Patterned Nickel Soft Lithographic Masters Using Aluminium Template. *Soft Nanosci. Lett.* **2011**, *1*, 41–45. [CrossRef]
67. Available online: http://www.verbatim.com (accessed on 15 September 2021).
68. Available online: http://intenso.de/index_en.php (accessed on 15 September 2021).
69. Available online: https://materialsproject.org/materials/mp-102 (accessed on 10 June 2021).
70. Available online: https://materialsproject.org/materials/mp-54 (accessed on 10 June 2021).
71. Proenca, M.P.; Merazzo, K.J.; Vivas, L.G.; Leitao, D.C.; Sousa, C.T.; Ventura, J.; Araujo, J.P.; Vazquez, M. Co nanostructures in ordered templates: Comparative FORC analysis. *Nanotechnology* **2013**, *24*, 475703. [CrossRef]
72. Available online: http://osta.org (accessed on 15 September 2021).